

Using Component Ratios to Detect Metadata and Instrument Problems of Seismic Stations: Examples from 18 Yr of GEOSCOPE Data

by Helle A. Pedersen, Nicolas Leroy, Dimitri Zigone, Martin Vallée, Adam T. Ringler, and David C. Wilson

ABSTRACT

Replacement or deterioration of seismic instruments and the evolution of the installation conditions and sites can alter the seismic signal in very subtle ways; therefore, it is notoriously difficult to monitor the signal quality of permanent seismic stations. We present a simple way to characterize and monitor signal quality, using energy ratios between each pair of the three components, as a complement to existing methods. To calculate stable daily energy ratios over a large frequency range (0.01–5 Hz), we use the daily median energy ratio over all 5 min windows within the day. The method is applied to all GEOSCOPE stations, for continuous BH channel data collected since 2001. We show applications to identify past gain problems (stations ROCAM and CRZF), to provide feedback after field interventions at remote sites (Antarctic station DRV), and to shed light on complex instrument problems (stations ECH and KIP). Our results show that component energy ratios have excellent time resolution and that they are visually simple for identification of problems. They can be used both for ongoing continuous monitoring of the signal quality, or as a tool to identify past problems. The Python code to produce the results in this work and the Python code for daily monitoring used by GEOSCOPE are available (see [Data and Resources](#)).

INTRODUCTION

Running high-quality seismic networks implies a constant monitoring of network performance (e.g., uptime, transmission) and data quality. Data quality issues can be separated into four main groups: orientation, timing, signal continuity, and signal quality (amplitude and fidelity). The present work addresses the issue of signal quality.

Seismic signals can be degraded in many ways. The noise level depends on location and installation conditions, but the signal can additionally have a number of issues such as mass-centering problems, glitches, increase in instrument self-noise, or faulty components. Most of these problems evolve or appear over time. In addition, the instrument response information,

that is, the information that makes it possible to convert the recorded counts to Earth units (displacement, velocity, or acceleration) may be erroneous. Many of these problems are frequency dependent. For example, as demonstrated by [Ekström *et al.* \(2006\)](#), the Streckeisen STS-1 broadband sensor instrument response may change, mainly at long periods, probably due to humidity ([Hutt and Ringler, 2011](#)). At very long periods, [Davis *et al.* \(2005\)](#) compared seismic recordings of radial mode ${}_0S_0$ (~ 1200 s period) and observed much larger amplitude variations than expected, some of the largest amplitude mismatch possibly being related to our ability to calibrate sensors at these long periods. In this very long-period range, [Davis and Berger \(2007\)](#) proposed to continuously monitor instrument performance using ocean tides, because major earthquakes that generate the global Earth resonance modes are too infrequent for routine monitoring. Although such methods are able to constrain the overall sensitivity, they might be unable to constrain information about the shape of the instrument response (e.g., 360 s corner on an STS-1).

An efficient way to monitor problems in field instruments is to detect changes between collocated sensors that operate in overlapping frequency bands. Such methods perform particularly well in the period band (~ 2 – 25 s) in which the microseismic noise provides a stable (barring seasonal changes) input signal ([Pavlis and Vernon, 1994](#); [Ringler *et al.*, 2010](#); [Ringler, Storm, *et al.*, 2015](#); [Casey *et al.*, 2018](#)). Comparison with collocated sensors of different types is also possible, for example, by comparing broadband and strong-motion signals under the condition that the input signal is of sufficient amplitude ([Kimura *et al.*, 2015](#); [Tasič, 2018](#)), even at relatively high frequencies (2–3 Hz, I. Tasič, personal comm., 2018). Nearby seismic sensors can also be used as a reference ([Langston, 2018](#); [Ye *et al.*, 2018](#)). In the absence of collocated or nearby sensors, an efficient, albeit resource-consuming, control method is to compare the permanent sensor with a well-calibrated portable sensor ([Davis and Berger, 2012](#)). Part of the system can be tested with calibration signals, in which the mechanically generated signal is replaced by a known electric signal (e.g., [Woodward and Masters, 1989](#); [Ekström and Nettles, 1997](#);

Ringler *et al.*, 2014). Using this method, a long-term assessment using such calibration signals was recently carried out for approximately 800 stations of the High Sensitivity Seismograph Network (Hi-Net) array by Ueno *et al.* (2015).

If no collocated or nearby sensors are available, network operators rely largely on monitoring the level of seismic noise, most often calculated as power spectral densities (PSDs). Using the probability density function (PDF) of many calculated PSDs, we can get statistical information about the frequency content (PDF, see also McNamara and Boaz, 2005). The PDFs are most often compared to high and low noise models (Peterson, 1993) to assess station performance. PDFs are, however, not well adapted to monitoring small changes because the noise level varies over several orders of magnitude (illustrated by the use of a decibel scale), both over time and as a function of frequency. We suggest adding a simple observation to the standard toolkit used by network operators for routine monitoring: the ratio of energy between each pair of the three components of motion. Our method is coherent with the event-based polarization analysis method suggested by Park and Ishii (2019), but it can also be used continuously, and over a wider frequency interval. Although the use of our method is limited to detecting inconsistencies between different components, it is very robust, easy to display and has an excellent time resolution. It can easily be included in software aimed at instrument monitoring and *a posteriori* information on data quality, such as Modular Utility for STatistical kNowledge Gathering (Casey *et al.*, 2018), Observatories and Research Facilities for European Seismology–European Integrated Data Archive (ORFEUS-EIDA) data quality tools, and the U.S. Geological Survey (USGS) Data Quality Analyzer (Ringler, Hagerty, *et al.*, 2015).

We test the concept on data from the GEOSCOPE network (Institut de Physique du Globe de Paris and École et Observatoire des Sciences de la Terre de Strasbourg [IPGP/EOST], 1982). The history of the GEOSCOPE program up to 2010 can be found in the historical overview of GEOSCOPE by Roult *et al.* (2010). The GEOSCOPE program was launched in 1981, with the explicit aim of increasing the global coverage of broadband stations. From the outset, GEOSCOPE (network code G) strived to distribute and share data widely and was an active partner in the creation of the International Federation of Digital Seismograph Networks in 1985 (Romanowicz and Dziewonski, 1987; Romanowicz, 1990) and in the establishment of ORFEUS in 1987. Because the declared scope of GEOSCOPE included global tomography and the Earth's resonance modes, the instrumentation was optimized for the recording of long-period signals. GEOSCOPE stations initially operated Streckeisen STS-1 seismometers only but presently also include Streckeisen STS-2 and Nanometrics Trillium 120PH and Trillium 240 sensors. The components of an STS-1 are independent sensors. Special care is taken at each site to ensure good coupling through the installation of the sensor on a granite plate (STS-2 and T240), on a warpless base plate (STS-1), or with the use of corundum (i.e., sand) in posthole installations (T120PH). Care is also

taken to protect the instruments from thermal, barometric, and magnetic field variations.

At all station visits and at installation, calibration of absolute gain is done using a collocated sensor that is laboratory calibrated. Electrical calibration, through the digitizer, is carried out by driving the calibration coil of the sensor. This enables the network operator to provide individual pole and zero response models for each component. Although this allows for very well-constrained response models, it also adds a source of error because of the excessive amount of bookkeeping to track individual response models for each component.

Routine monitoring of instrument performance is carried out with PDFs and comparison with synthetic data for large earthquakes. At some sites, additional state of health data (e.g., room temperature, barometric pressure, and humidity) is also recorded to facilitate remote trouble shooting. Since February 2019, routine monitoring of GEOSCOPE stations now includes energy component ratios as suggested here.

Continuous data storage and distribution started in 1984 on the VH channel for a few GEOSCOPE stations. Data from a few VH channels were distributed as early as 1984, and migration to a systematic distribution of continuous BH data started in the 1990s. In this work, we report on an analysis of continuous GEOSCOPE data. The entire data analysis was carried out on the BH channel only, starting in 2001.

DATA ANALYSIS

All GEOSCOPE stations over the period 2001–2019 were analyzed, and examples, which demonstrate different uses of the method, are shown and discussed in the Results section. The data analysis is applied on daily files with the three components of the BH channels. The BH channels correspond to seismic broadband sensors, with (for GEOSCOPE stations) 20 Hz sampling rate. We subsequently analyze daily data only if there is a continuous data stream within the day covering at least 96% of the day (i.e., ~83,000 s). This limit can be applied in the case of high-quality data streams such as validated GEOSCOPE data; however, it can be relaxed for near-real-time data or stations with data gaps.

Data preprocessing is standard: demean, detrend, taper (cosine taper over 5% of the signal length), and removal of instrument response. BH1 and BH2 components are rotated into north and east components. In the present work, we analyze data in frequency bands up to 5 Hz. For studies focusing on lower frequencies, for example, for daily monitoring purposes using the second microseismic peak, it is preferable to downsample the data to speed up the preprocessing and the analysis.

The observed parameters are daily ratios (E/Z, N/Z, and E/N) of squared amplitudes of each component. The measurement is deceptively simple, but some caution still needs to be taken. First, the ratios must cover the same time interval (within the uncertainty of half the duration of the sample interval). Second, the effect of outliers must be minimized. Indeed, spikes, local noise, and earthquakes may significantly

change the average daily energy level on one or several components, especially outside the first and second microseismic peaks. In particular, long-period component ratios generally have large scatter if we calculate the daily component ratios using the average daily energy of each component. We therefore adopt an alternative approach, using median energy ratios calculated over a large number of time windows. The shorter the time window, the higher the number of windows over which the median is calculated, thereby increasing the stability of each daily component ratio. To allow for a minimum number of three periods within the time window, we use a window length of 300 s (corresponding to three periods of 100 s, which is our longest period analyzed), making it possible to calculate the median value over 288 time windows if there are no gaps in the daily file.

Processing for each station is as follows: For each day we

- download daily files of BH channels and preprocess (see above);
- filter in target frequency bands (third-order Butterworth, zero phase). The frequency bands are: 0.01–0.02, 0.02–0.05, 0.05–0.1, 0.1–0.2, 0.2–0.4, 0.4–1, 1–2, and 2–5 Hz;
- cut data into 5 min windows. If the data segment for each component is longer than 294 s (98% of 5 min window), calculate the average energy (i.e., sum of squared amplitudes divided by the number of samples) on each component;
- calculate energy ratios (N/Z, E/Z, and E/N) between the components in each 5 min window; and
- calculate the daily energy ratio of each of the three energy ratios as the median over all the 5 min time windows.

A faster algorithm is to use the mean over the longest daily data segments. In that case, the measurements are stable mainly within the frequency windows that correspond to the first and second microseismic peaks.

The Python code used to produce the figures of this article and a Python code for daily monitoring are freely available (see [Data and Resources](#)).

RESULTS

Examples of Gain Problems at Stations ROCAM and CRZF

GEOSCOPE station ROCAM (latitude $\sim -19.8^\circ$, longitude $\sim 63.4^\circ$), located in the Leguat Reserve on Rodrigues Island (Republic of Mauritius) in the Indian Ocean, started operating in 2012. The sensor, a Streckeisen STS-2, is installed in a natural cave located 1 km from the coast. Figure 1 shows the energy ratio between the east–west component and the north–south component over a period of four years. The black points show the component ratios using the response files available prior to February 2019. The E/N energy ratio suddenly increases (by a factor of approximately 4) at the beginning of 2016 and returns to its initial value in summer 2017. A similar problem occurs at the end of 2018. At the same time, the N/Z energy ratio (not shown here) decreases by approximately the same factor in all frequency bands, whereas the E/Z ratio is not

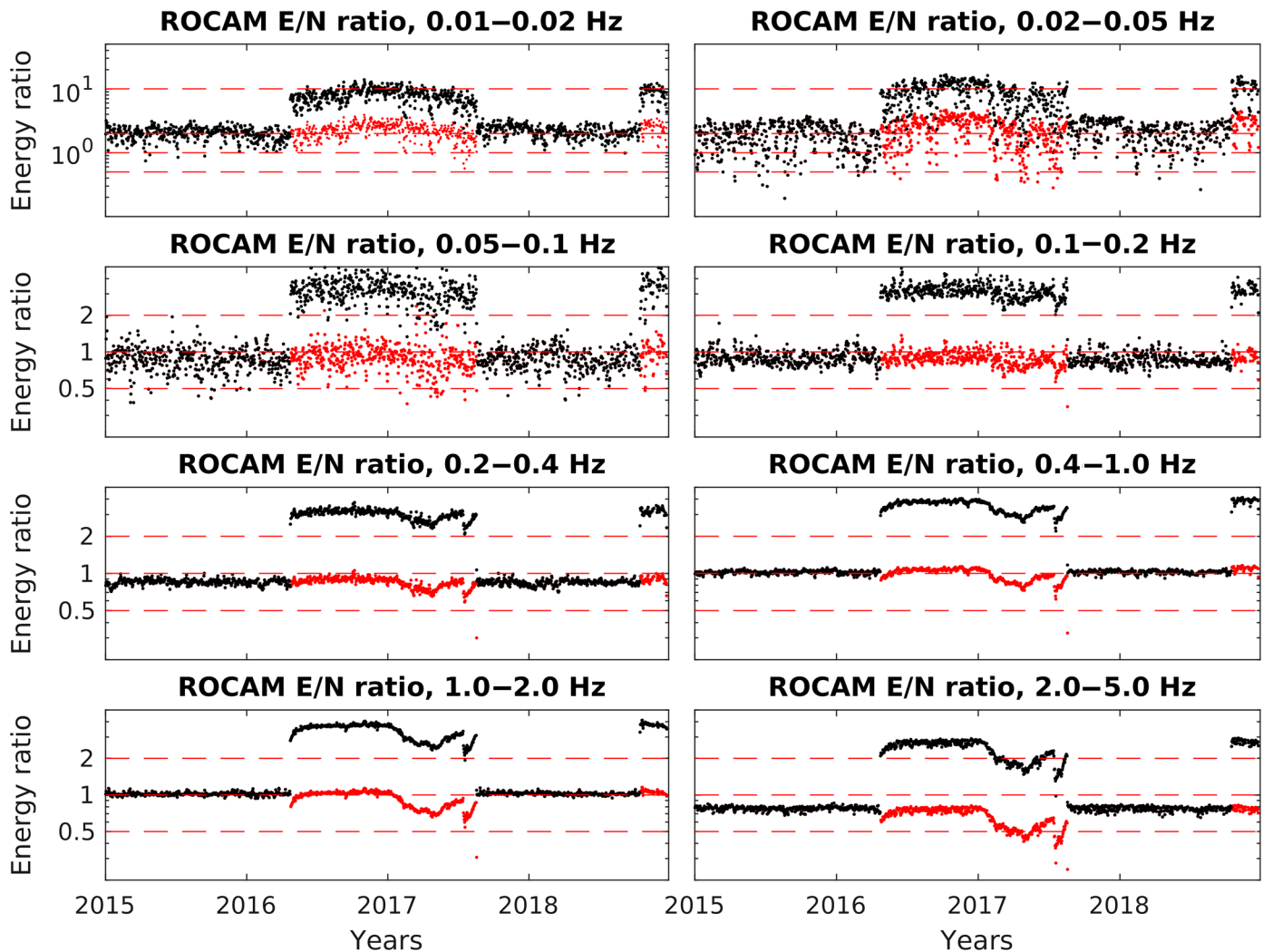
affected. Further analysis of the data made it possible to identify a temporary erroneous gain on the north–south component, probably due to a cable problem or a preamp electronics failure, which reduced the signal amplitude by a factor of 2. After correcting the sensitivity in the instrument response file for the north component, there is no major remaining gain issue on any of the energy component ratios, as illustrated by the red dots in Figure 1. The correction was also applied from the end of 2018 and onward, based on the analysis of component energy ratios.

GEOSCOPE station CRZF (latitude $\sim -46.4^\circ$, longitude $\sim 51.9^\circ$) is located on the very remote Ile de la Possession, in the Crozet archipelago, located midway between Madagascar and Antarctica. It is accessible for maintenance once a year, by boat only, during the logistical tour of all French Southern Territories. The station, installed in 1986, is equipped with a Streckeisen STS-1 sensor, which is located in a partly buried hut in soft soil. The energy component ratios (Fig. 2) show that this station cumulates several problems. At long periods, we observe an anomalously high E/N ratio, which additionally has strong seasonal variations, demonstrating that the two components do not have the same response to seasonal changes. This problem, along with the strong seasonal variations, disappeared after a field intervention on 14 April 2016 during which the old STS-1 feedback electronics were replaced with a Metrozet E300 feedback electronic system. We refer to the section, example of complex instrument problems at ECH, for further discussion of component ratios at long period. In addition, the station has a probable gain problem on the east–west component between 17 March 2014, and 14 April 2016. Indeed, this problem can be identified in all frequency intervals except the lowermost ones, in which the sudden change cannot be reliably identified within the strong scatter and seasonal variations of the component ratios. At the time of writing (September 2019), the GEOSCOPE team considers it likely that there is a gain issue—approximately 40% lower on the east–west component—related to a cable problem or a preamp electronics failure.

Example of Station Repair at Antarctic Station DRV

GEOSCOPE operates two broadband seismic stations in Antarctica. Updates and repairs happen at best once a year, during the Antarctic summer campaigns, where the station operator stays on site for 4–5 weeks. Travel to the two sites from the Antarctic basecamp takes approximately seven days depending on the weather conditions and the means of transport (boat or plane). It is therefore crucial that the efficiency of field interventions is checked immediately, before the personnel leaves the site on predefined dates.

On 6 February 2010, the GEOSCOPE team carried out a major operation on station DRV (latitude $\sim -66.7^\circ$, longitude $\sim 140.0^\circ$), which is located at the Dumont d'Urville scientific base. At this site, strong reduction of the primary and secondary microseismic energy is observed during the winter due to the presence of sea ice, resulting in strong annual variations of the seismic noise (e.g., [Grob et al., 2011](#)). The reinstallation of the station was necessary because the STS-1 east–west component



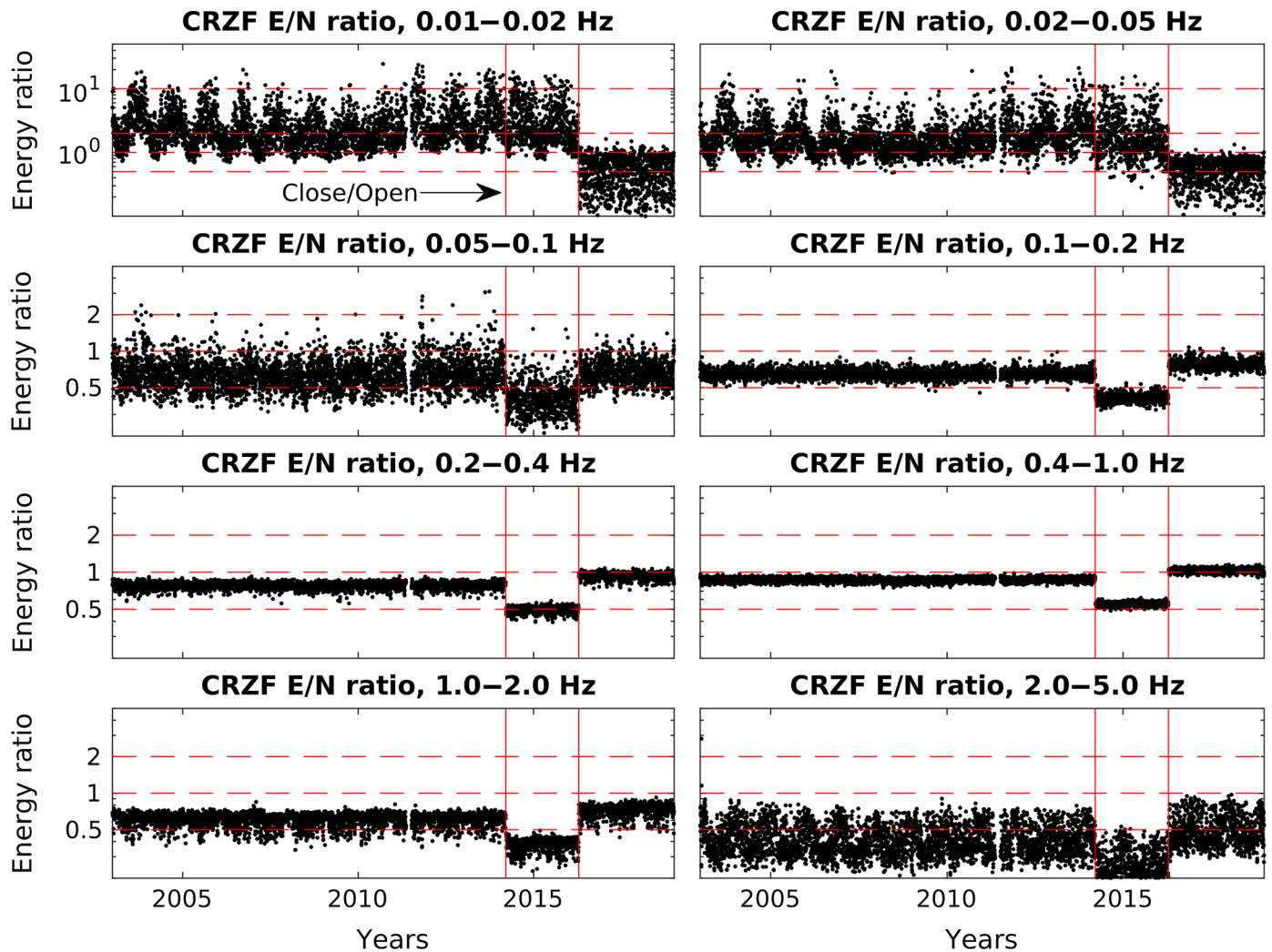
▲ **Figure 1.** Daily median energy ratios between the east–west and the north–south components for station ROCAM, in eight frequency bands (indicated above each plot). Note that the energy ratio scale ranges from 0.1 to 50 at low frequency (top plots) and from 0.2 to 5 in the other frequency bands. The red (gray in printed version) dots correspond to component ratios after correction for erroneous gain on the north component between 23 March 2016 and 18 July 2017, and after 15 September 2018. The black dots overlay the red (gray) ones during the periods in which the instrument response has not changed. Before correction, there was no closing and opening of channels during the period plotted here, whereas the new instrument response has channel openings and closings for the north component on the three dates indicated earlier. The color version of this figure is available only in the electronic edition.

had recurring problems after mechanical damage on the electronics on 22 August 2008. The damage on the east component is visible in Figure 3 with a clear drop on the E/N ratio. The DRV station was consequently switched to an STS-2 sensor on 6 February 2010. Figure 3 demonstrates that the effect of the repair is easily detected with the component ratios. Figure 4 shows the same data, for the two lowest frequency bands and with a time zoom on the day of the intervention ± 30 days. The effect of the repair is immediate on this component ratio and at long periods and would have been valuable additional information at that time for the field crew. In addition, we observe a decrease in annual variations of component energy following the change of instrument, both in the two lowermost and the uppermost frequency bands. Strong seasonal variations are also present on the E/Z

ratio, but not on the N/Z ratio, indicating that the east component was the most affected by these annual variations.

The DRV station was switched back to the original STS-1 sensor, this time with Metrozet E300 feedback electronics, on 1 January 2013 (second red vertical line in Fig. 3). This complete reinstallation did not increase the annual variations to previous levels, leading us to conclude that installation conditions, or the old STS-1 electronics, led to strong seasonal variations on the east component for the initial installation.

Example of Complex Instrument Problems at Station ECH
ECH (latitude $\sim 48.2^\circ$, longitude $\sim 7.2^\circ$) is located in the Vosges, on the edge of the French side of the Rhine graben, close to Strasbourg. It is installed in a narrow gallery of a silver



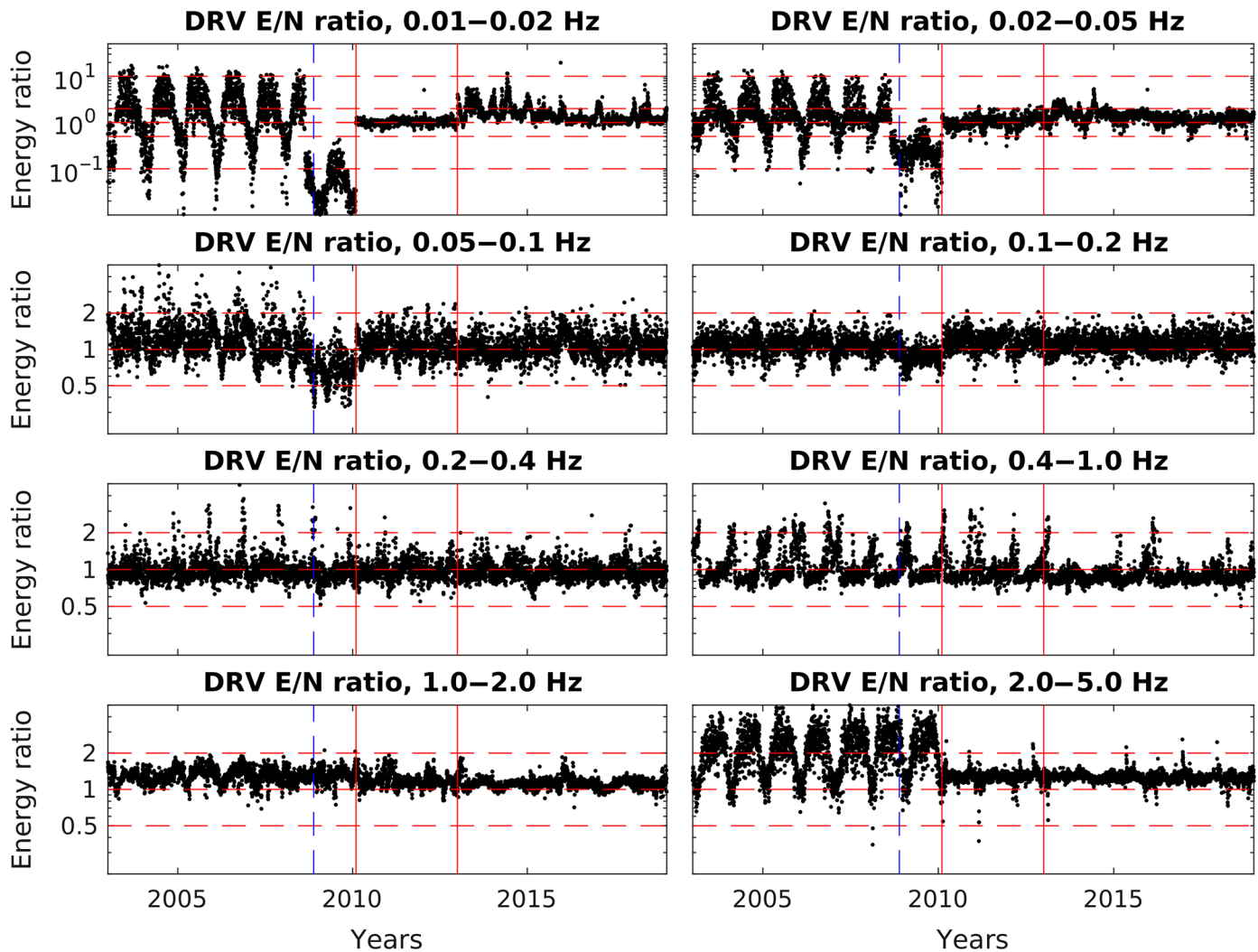
▲ **Figure 2.** Daily median energy ratios between the east–west and the north–south components for station CRZF, in eight frequency bands (indicated above each plot). Note that the energy ratio scale ranges from 0.1 to 50 at low frequency (top plots) and from 0.2 to 5 in the other frequency bands. The vertical red (gray in printed version) lines correspond to days of closing and opening channels. The E/Z energy ratio decreases during the same time period as the E/N energy ratio, whereas the N/Z energy ratio is stable. The color version of this figure is available only in the electronic edition.

mine from the Middle Ages. Because of its location in metropolitan France, with good connectivity and easy access, it has a very high level of data continuity. Continuous data streams are available for ECH since 1990. We here focus on continuous BH data from 2015. The instrumentation since October 2002 has been stable, with a Streckeisen STS-1 and its legacy feedback electronics until 29 July 2015, followed by installation of Metrozet E300 electronics associated with the STS-1 from 29 July 2015 onward. At this field intervention, the sensors were moved ~ 20 m and each installed on a warpless base plate to decrease long-period noise. In addition, the digitizer was moved closer to the sensor, reducing the sensor-digitizer cable from approximately 300 m to a few meters.

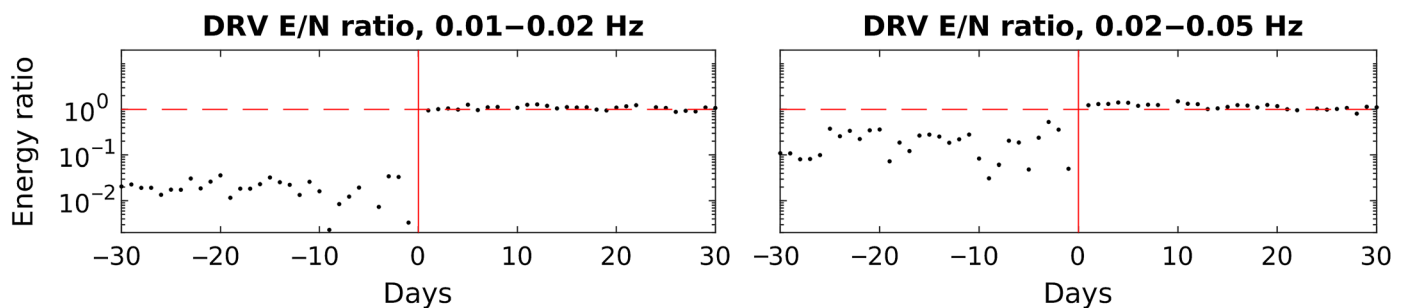
Figure 5 shows PSD functions on the three components, for years 2014 and 2016, that is, before and after the reinstallation in 2015. ECH is installed in a high-quality site, with the

vertical PDFs close to the low-noise model. The PDFs on the vertical component hardly changed between 2014 and 2016, whereas the spread of the PDFs on the horizontal components was reduced at long periods. Careful inspection demonstrates no major obvious change on the horizontal components between 2014 and 2016, but hints at a potential increase in noise level at low frequencies on the east–west component.

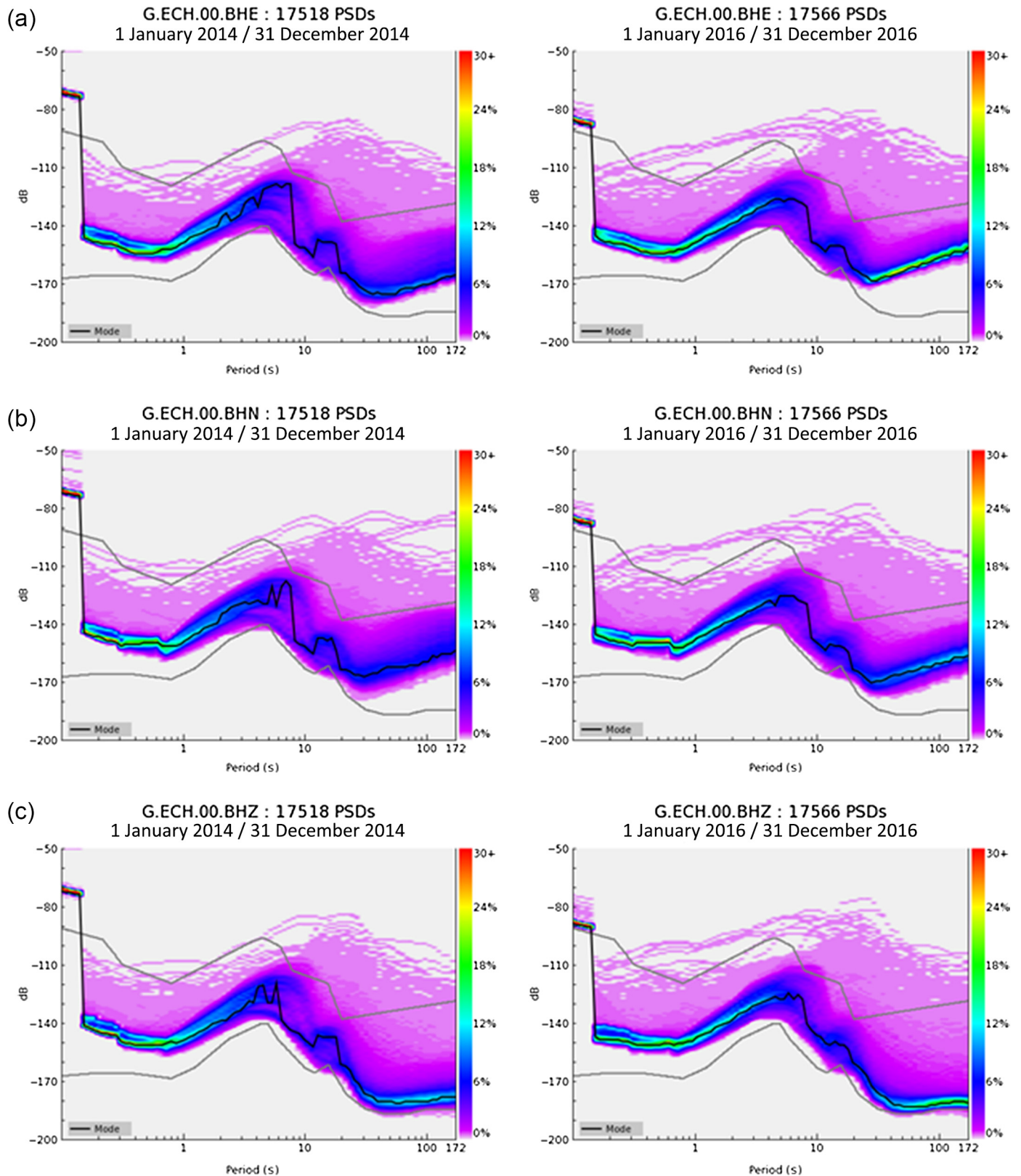
Figures 6–8 show the component ratios in all frequency bands, for component ratios E/Z, N/Z, and E/N. For clarity, the vertical scale is different between the lowermost two frequency bands and the other frequency bands, and between horizontal-to-vertical component ratios and E/N ratios. The vertical red line shows the day of the reinstallation (29 July 2015). Looking first at frequency band 0.1–0.2 Hz (second microseismic peak), we observe that the ratio of horizontal components to the vertical component (Figs. 6, 7) is approximately



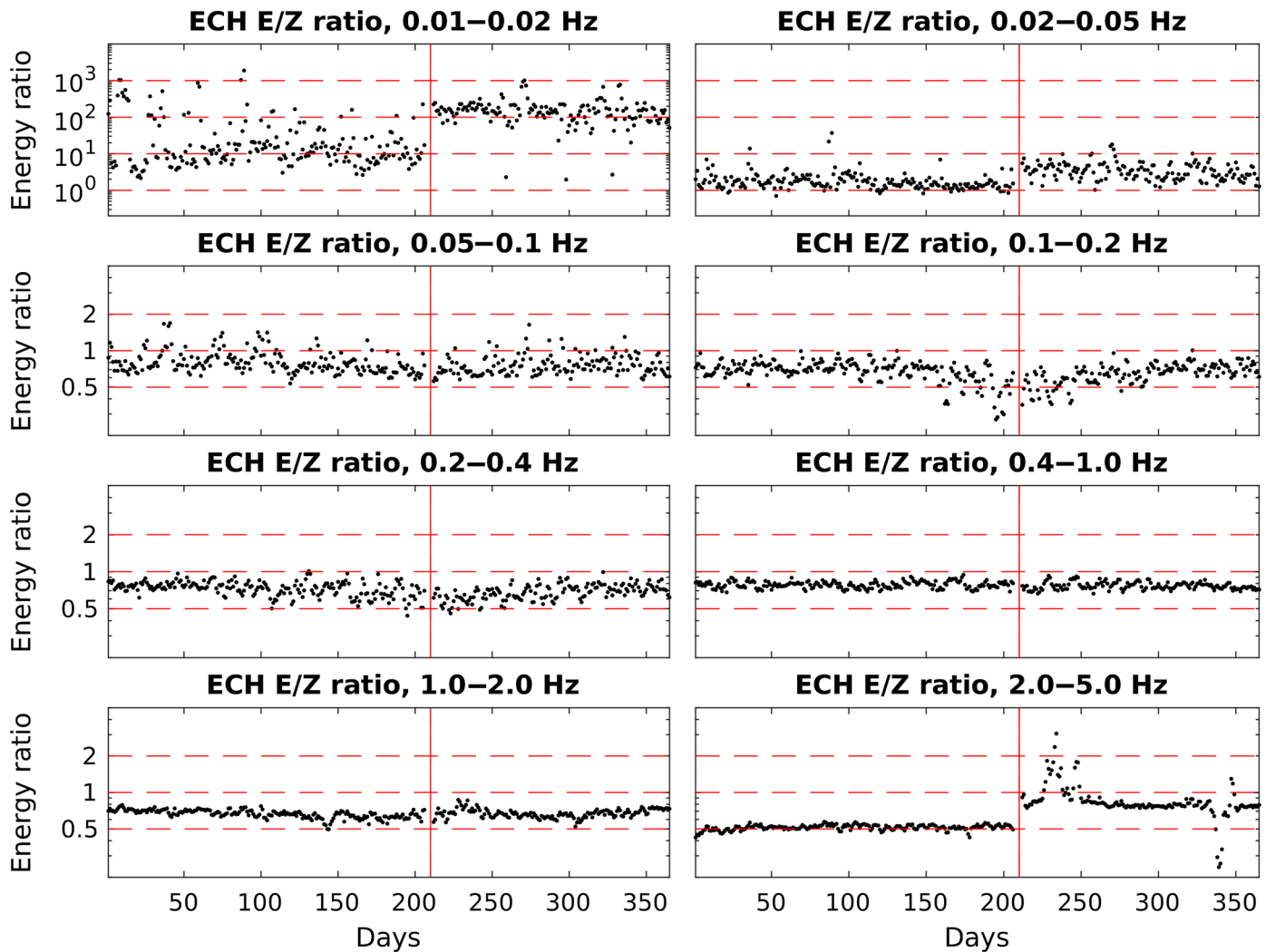
▲ **Figure 3.** Daily median energy ratios between the east–west and the north–south components for station DRV, in eight frequency bands (indicated above each plot). Note that the energy ratio scale ranges from 0.01 to 50 at low frequency (top plots) and from 0.2 to 5 in the other frequency bands. The vertical red (gray in printed version) lines correspond to days of closing and opening channels. The vertical blue (gray in printed version) dashed line corresponds to the date of mechanical damage to electronics. The color version of this figure is available only in the electronic edition.



▲ **Figure 4.** Same as Figure 3, for the two lowest frequency bands, in a time window covering 30 days before to 30 days after the intervention on 6 February 2010, here set to time 0. The vertical scale is adapted to the zoom (0.002–20). The color version of this figure is available only in the electronic edition.



▲ **Figure 5.** Power spectral density (PSD) functions (McNamara and Boaz, 2005) for (a) BHE, (b) BHN, and (c) BHZ components of ECH (location 00) in 2014 (left) and 2016 (right). The color version of this figure is available only in the electronic edition.



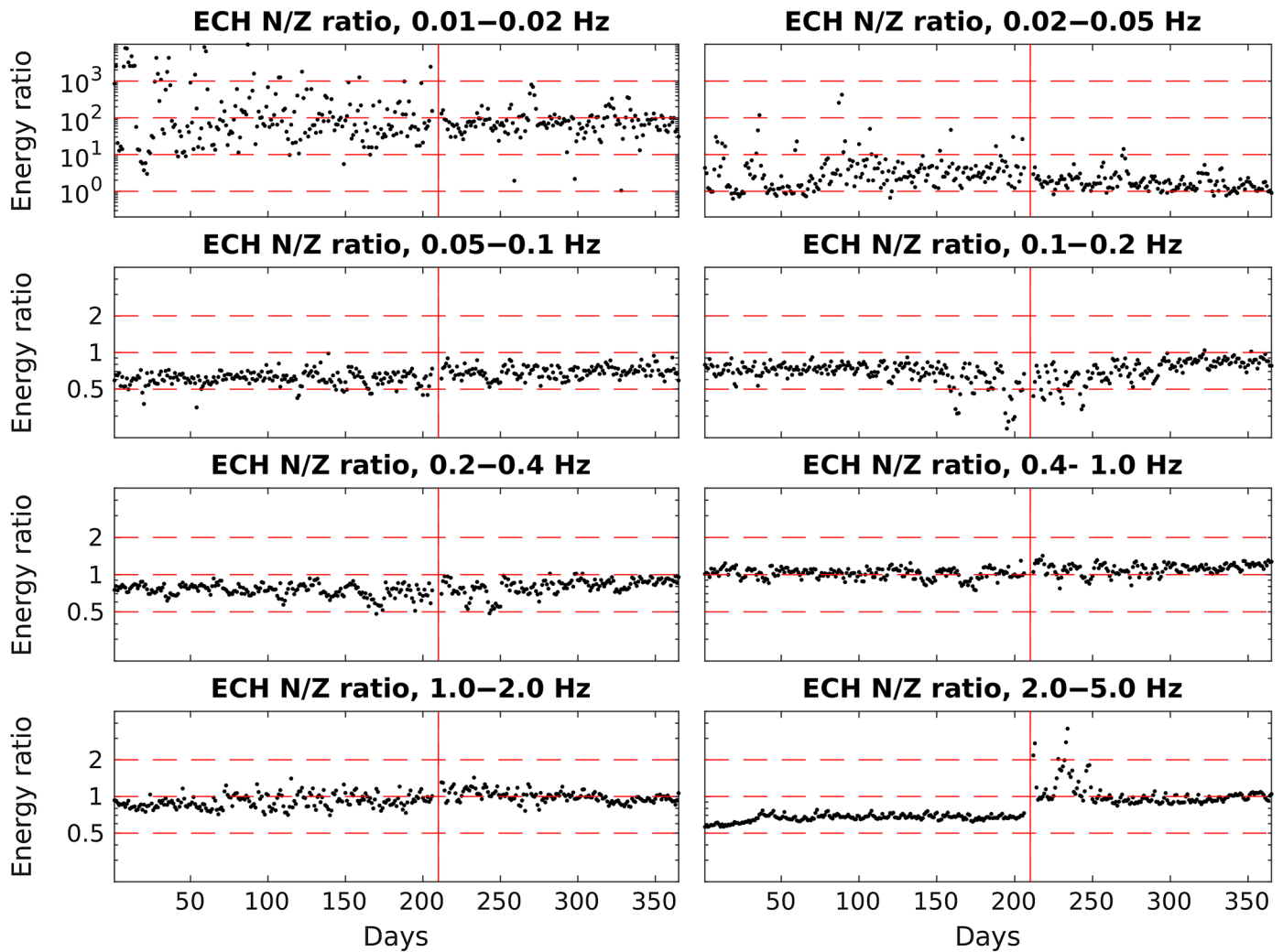
▲ **Figure 6.** Year 2015 daily medians of energy ratios between the east–west and the vertical components for station ECH, in eight frequency bands (indicated above each plot). Note that the energy ratio scale ranges from 0.1 to 10000 at low frequency (top plots) and from 0.2 to 5 in the other frequency bands. The vertical red (gray in printed version) line corresponds to the day of the reinstallation on 29 July (day 210) 2015. The color version of this figure is available only in the electronic edition.

stable at ~ 0.7 – 0.8 over the whole year, for both components, with a decrease in E/Z and N/Z ratios over the summer months. This decrease is observed at station ECH for all the years analyzed as well as for other stations in metropolitan France and must, therefore, be attributed to changes in the composition of the seismic noise. The ratio between the horizontal components (E/N ratio, Fig. 8) is ~ 1 before the field intervention and approximately 0.9–0.95 afterward. This would correspond to an error of approximately 2%–5% in signal amplitude on one of the components either before or after the instrument upgrade. Similar conclusions can be drawn in all the intermediate frequency bands, ranging from 0.05–0.1 Hz up to 0.4–1.0 Hz, possibly even up to the 1.0–2.0 Hz frequency band.

In the frequency band 2–5 Hz, both of the horizontal-to-vertical ratios change significantly on 29 July 2015, with an increase from ~ 0.5 to 0.8 for E/Z and an increase from ~ 0.7 to 1 for N/Z. In addition, August shows high E/Z and

N/Z ratios, which would be related to either a decrease in energy on the vertical component, or an increase on both horizontal components. This period corresponds to the main period of tourist activity in this isolated site, with guided tours in silver mine tunnels close by, so a change in the noise characteristics cannot be excluded. There is also a sudden drop and fast recovery on the E/N and E/Z ratios at the end of the year. In this frequency interval, the ratios are overall dominated by a periodicity of seven days (except for the anomalies at short periods previously described), that is, dominated by anthropogenic noise. Further investigation may enable us to identify possible errors in the high-frequency poles either before or after 29 July 2015.

Bigger changes appear at low frequency (0.01–0.02 Hz). The E/N ratio, which we expect to be approximately one, increases from ~ 0.14 before the field intervention, to ~ 2 afterward, whereas the E/Z ratio increases from ~ 10 to ~ 100 . The



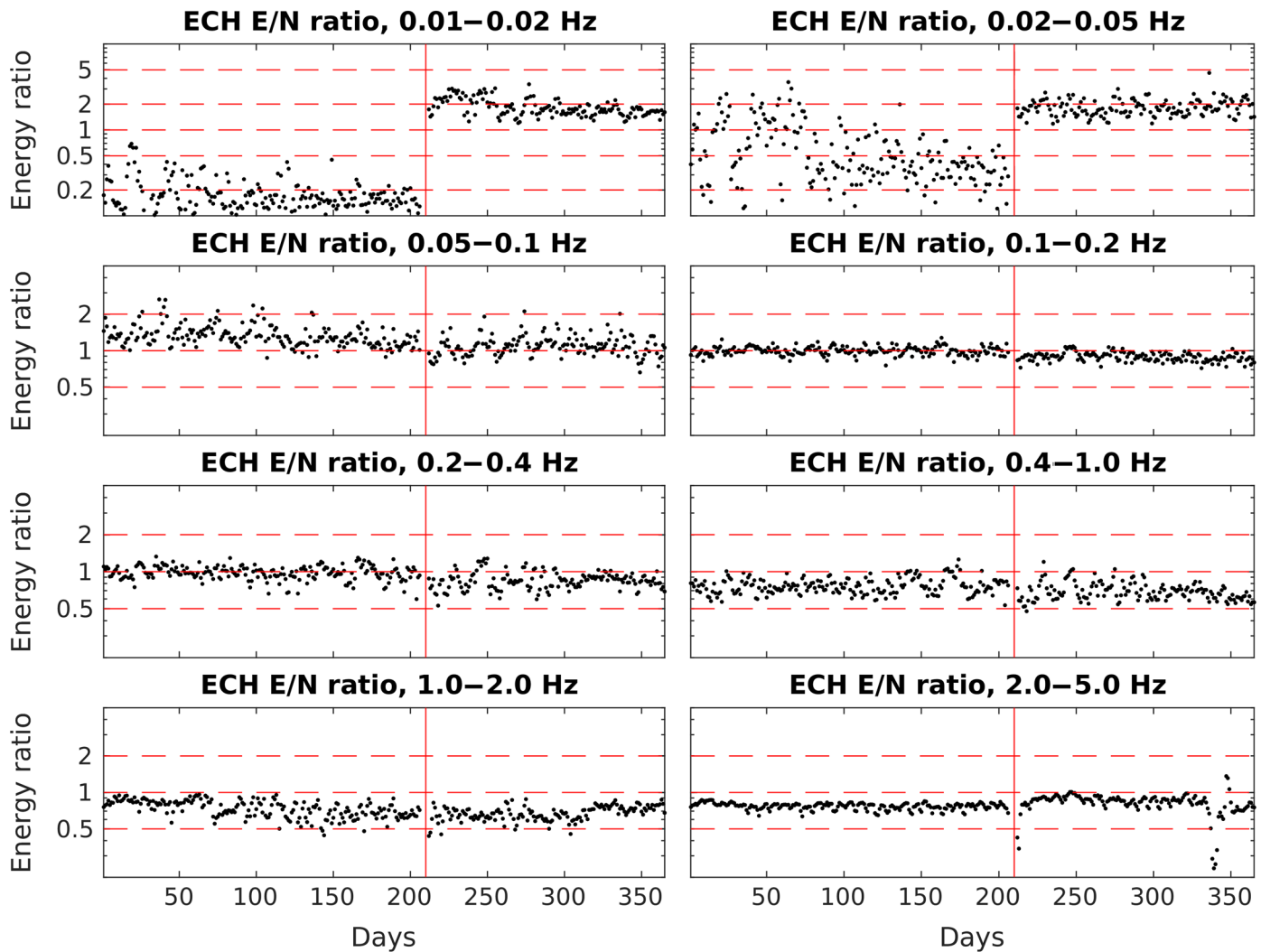
▲ **Figure 7.** Year 2015 daily medians of energy ratios between the north–south and vertical components for station ECH, in eight frequency bands (indicated above each plot). Note that the energy ratio scale ranges from 0.1 to 10000 at low frequency (top plots) and from 0.2 to 5 in the other frequency bands. The vertical red (gray in printed version) line corresponds to the day of the reinstallation on 29 July (day 210) 2015. The color version of this figure is available only in the electronic edition.

N/Z ratio does not overall change, but the scatter is significantly reduced after the sensor reinstallation. Similar effects, but smaller, are observed in the frequency interval 0.02–0.05 Hz. This means that the N component did not change in amplitude, but the sensor reinstallation improved the overall behavior of the N component (also seen in the PDF). The difference between the E/Z and N/Z ratios indicates significantly different behavior of the two components. Combining the information with those of the PDFs, it would appear that the E/N ratio after the reinstallation stabilized mainly because of an increase of the noise level on the east–west component.

Figure 9 shows the three component ratios in the lowermost and uppermost frequency bands, for five magnitude > 7 earthquakes in 2014–2016 for which the theoretical back azimuth is approximately 45° . In this figure, we show all 5 min windows, within a duration of ± 5 hr before and after the event time t_0 . Using such a long window after the earthquake

means that the data after t_0 are dominated by coda waves, that is, the energy ratios should not be strongly influenced by the radiation pattern.

In the lowermost frequency band, we observe that earthquakes before (black dots in Fig. 9) and after (red dots in Fig. 9) July 2015 have almost (scatter excluded) the same component ratios. In particular, the E/N ratios at low frequencies demonstrate that, although the noise ratios are different before and after July 2015, the earthquake signal does not change over time. This observation excludes instrument response errors and is coherent with the hypothesis that the reinstallation increased the noise levels on the east–west component. On the contrary, at high frequencies, there is a change in the ratio of horizontal-to-vertical components, which is independent of the amplitude of the signal. A possible cause could be erroneous instrument response, at high frequency, for both horizontal components, or for the vertical component, indicating that recalibration



▲ **Figure 8.** Year 2015 daily medians of energy ratios between the east–west and the north–south components for station ECH, in eight frequency bands (indicated above each plot). Note that the energy ratio scale ranges from 0.1 to 10 at low frequency (top plots) and from 0.2 to 5 in the other frequency bands. The vertical red (gray in printed version) line corresponds to the day of the reinstallation on 29 July (day 210) 2015. The color version of this figure is available only in the electronic edition.

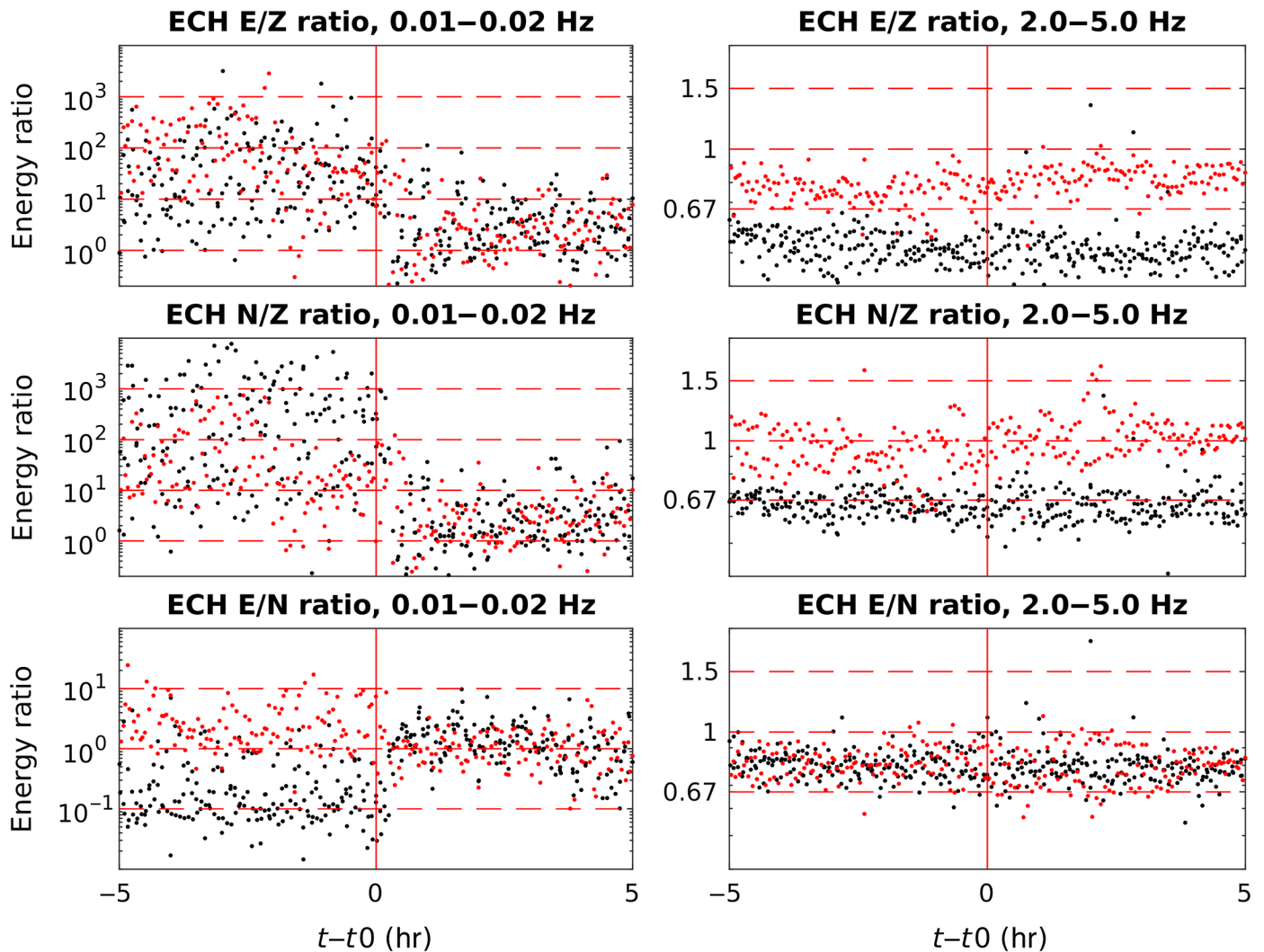
should be carried out. Using a laboratory-calibrated mobile sensor will enable us to test the high-frequency performance.

Example of Component Energy Ratios and Collocated Sensors Comparison at Station KIP (Network Code Shared G and IU)

Station KIP (latitude $\sim 21.4^\circ$, longitude $\sim -158.0^\circ$) in Hawaii, U.S.A., is a shared station between Global Seismographic Network (GSN) and GEOSCOPE networks and is installed on concrete piers inside a tunnel cut in the side of a canyon of basalt. Data are distributed under network codes G and IU (Albuquerque Seismological Laboratory/U.S. Geological Survey [ASL/USGS], 1988). The issues reported here are identical under both network codes as they refer to the same instrument and recording equipment. BH data from KIP location code 00 (or no location code) are available since August 1988, first with a Streckeisen STS-1 seismometer with original

Streckeisen STS-1 feedback electronics. On 18 August 2010, the Streckeisen STS-1 feedback electronics were replaced with a Metrozet feedback electronics box. Finally, on 29 June 2018, a Streckeisen STS-6A was also deployed at this station. Data from location code 10 are available since February 1999, with a Streckeisen STS-2 seismometer until 22 March 2012. Later, this sensor was replaced with a Streckeisen STS-2.5, which is currently the running location code 10. Because of operations in a humid environment, maintenance operations occur frequently, with, for example, new feedback box electronics of the STS-1 on 26 May 2006. In August 2010, the feedback electronics were again replaced, and the digitizer was changed (from Quanterra Q680 to Q330). Further details on instrumentation and installation of KIP can be obtained from the Albuquerque Seismological Laboratory, USGS.

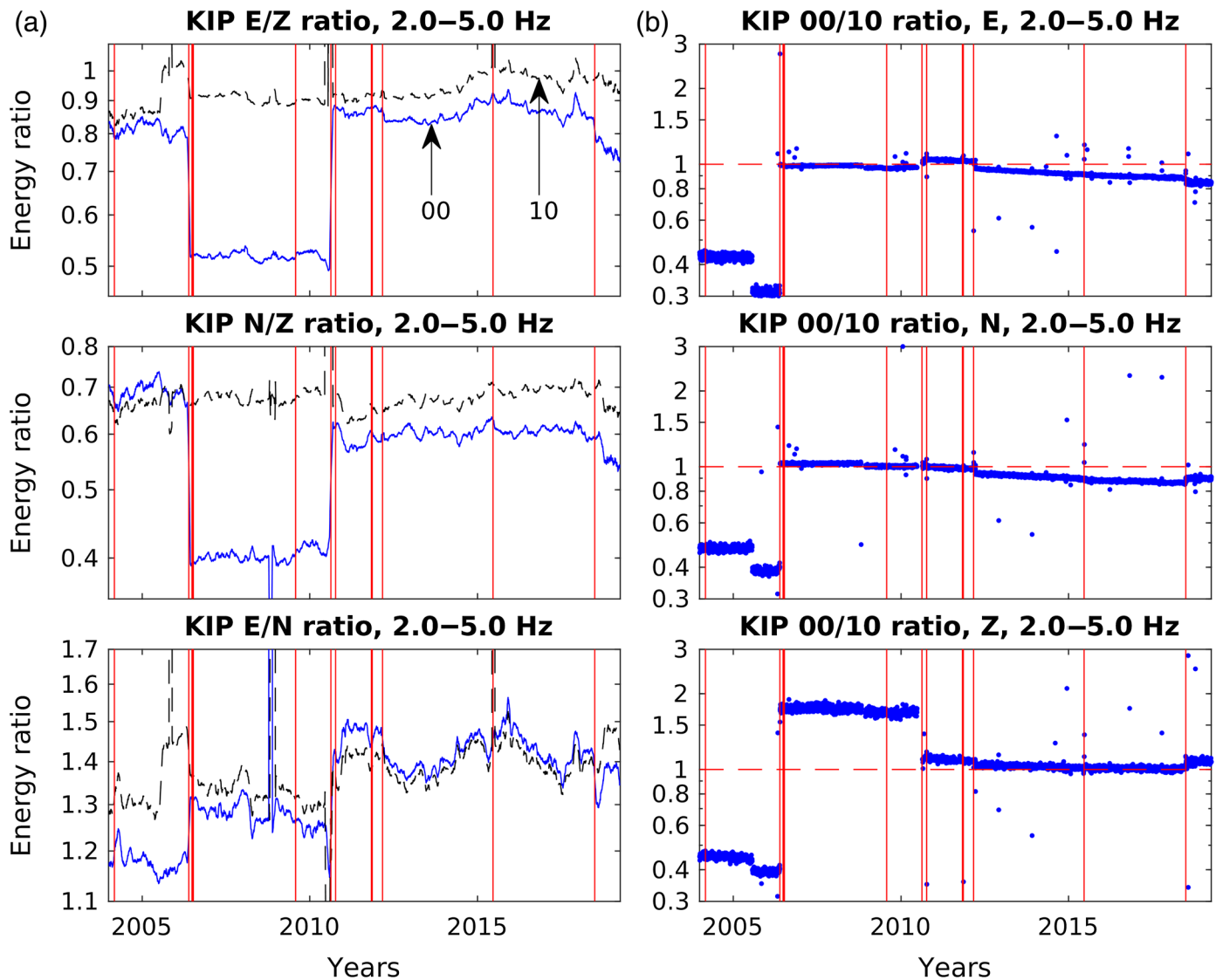
Because KIP has two collocated instruments, it affords the opportunity to compare the component ratios with the ratios



▲ **Figure 9.** Component energy ratios at ECH in five 10 hr periods each containing a major earthquake (magnitude > 7) in 2014–2016, with theoretical backazimuth at approximately 45° . Energy ratios shown for all the 5 min (nonoverlapping) windows. Black dots show energy ratios for 10 hr time windows around three earthquakes prior to July 2015, and red (gray in printed version) dots show data energy ratios for 10 hr time windows around two earthquakes after July 2015. The timescale shows $t - t_0$, in which t_0 is the event time. Note that the vertical scale differs between the two frequency bands and, at long period, between horizontal to vertical ratios and E/N ratios. The color version of this figure is available only in the electronic edition.

of energy for identical components at the station. For the 00/10 ratios, we use the same processing as for component ratios, the only difference being that we calculate energy ratios of the same component at the two locations (00/10). Our 00/10 energy ratios in the second microseismic peak correspond closely to the method suggested by Ringler, Storm, *et al.* (2015). As demonstrated by these authors, collocated sensors may have stronger differences than those predicted by the uncertainty in instrument response, and it is not always possible to pinpoint which of the two sensors is at fault when the signals differ slightly (Ringler, Storm, *et al.*, 2015). To better compare the observations (component ratios and location ratios), we further reduce the scatter in the component ratios by applying a sliding window of 30 days. The 00/10 ratios are overall very stable; therefore, no smoothing over time was needed.

We show the comparison of data from the two locations, in two frequency intervals, 0.2–0.4 Hz and 2–5 Hz. For the high frequencies (Fig. 10), we first focus on the period between May 2006 and August 2010. In May 2006, the 00/10 ratios increase abruptly to ~ 1.7 for the Z component. At location 00, the E/Z ratio decreases abruptly in May 2006 from ~ 0.9 to 0.55 and the N/Z ratio from ~ 0.7 to 0.4. Taken together, these imply that the jump in the 00/10 ratio of the Z component has its origin at location 00. This problem is not present at longer periods (see Fig. 11); therefore, a tentative explanation is an error in the high-frequency pole of the vertical sensor of the STS-1 seismometer. Some other GEOSCOPE stations equipped with STS-1 sensors also show issues at high frequency. This observation can probably be explained by the fact that even small errors in the high-frequency poles can lead to significant

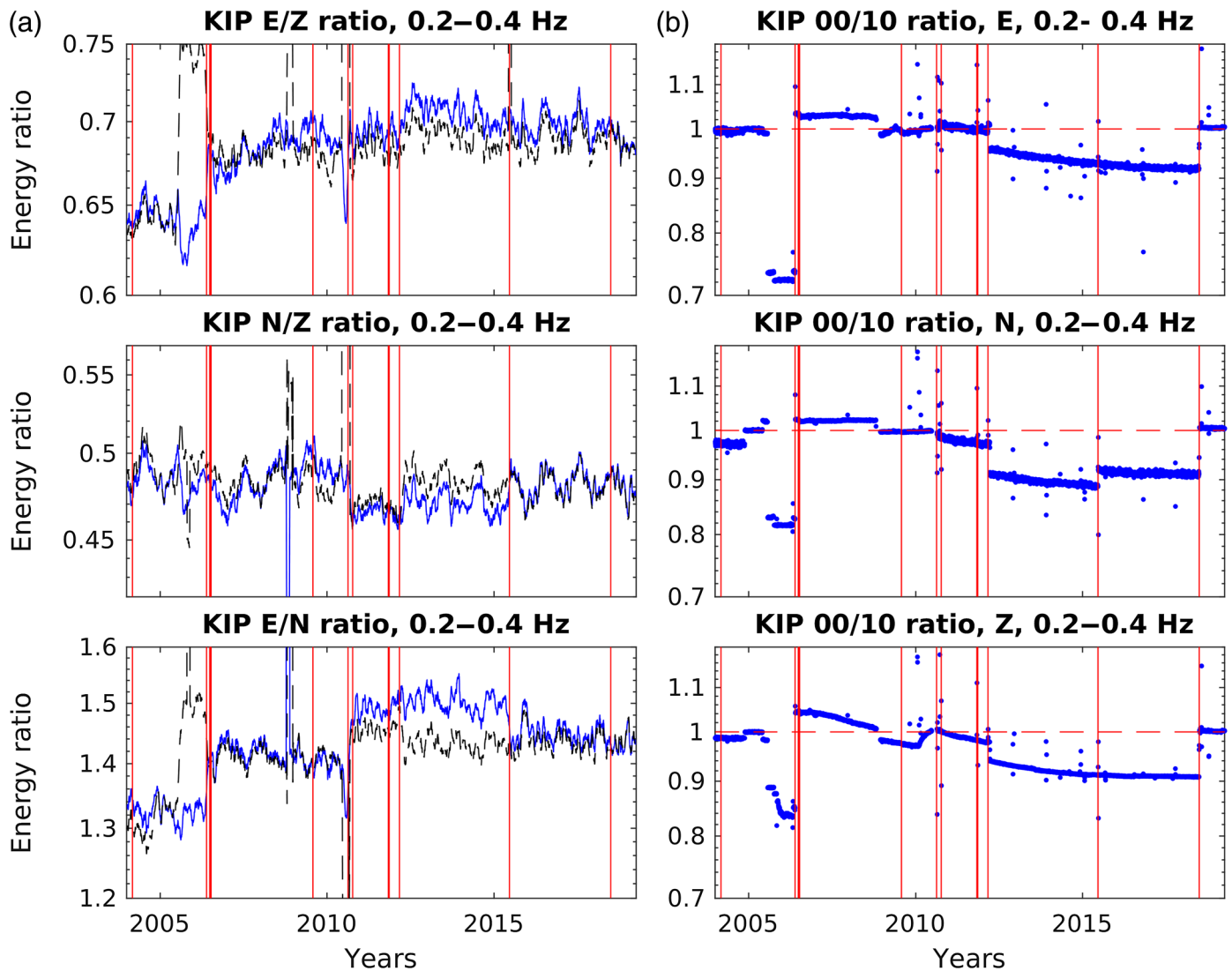


▲ **Figure 10.** Energy ratios between components and locations in frequency band 2–5 Hz for station KIP (network codes IU and G). (a) Daily median energy ratios between all components (E/Z, top; N/Z, center; and E/N, bottom). Solid line indicates location 00. Dashed line represents location 10. (b) Energy ratios for same components at location 00 and location 10, using components (top) E, (center) N, and (bottom) Z. The vertical red (gray in printed version) lines correspond to days of closing and opening channels in any of the two locations and for any BH channel. The color version of this figure is available only in the electronic edition.

amplitude errors in the 2–5 Hz frequency interval, because the high end of this frequency interval is close to the pole. Immediately prior to May 2006, there is a period of several months with high E/Z and E/N component ratios at location 10. At the same time, the 00/10 ratios are down to ~ 0.3 for the E, and ~ 0.4 for the N and Z components. For that period, one can tentatively point toward problems on the east component at location 10, but this occurs on top of the problems present previously. It would be useful to revisit calibration signals for that period to verify whether the high-frequency poles at that time are correct for the two sensors and for each component. After 2010, there is a slow decrease of the 00/10 ratios for E and N components, coherent with differences in E/Z and N/Z ratios for the two locations. Although it is not straightforward

to identify which of the two locations is problematic, one can tentatively suggest an aging problem of one of the instruments, or, alternatively, changes in local conditions of anthropogenic noise or changes in the piers, which could influence the observations at high frequencies.

At 0.2–0.4 Hz, that is, within the band of microseismic noise, we also observe slow changes in 00/10 ratios after 2015 but this time with almost identical component ratios at the two locations. We do, however, observe that the anomalous behavior observed at high frequency in 2005 on the E/N and E/Z ratios (Fig. 10) is also present in the frequency interval 0.2–0.4 Hz. This problem is present in all the frequency intervals, pointing toward a possible gain problem at location 10 during that time.



▲ **Figure 11.** Energy ratios between components and locations in frequency band 0.2–0.4 Hz for station KIP (network codes G and IU). (a) Daily median energy ratios among all components (E/Z, top; N/Z, center; and E/N, bottom). Solid line indicates location 00. Dashed line represents location 10. (b) Energy ratios for same components at location 00 and location 10, using components (top) E, (center) N, and (bottom) Z. The vertical red (gray in printed version) lines correspond to days of closing and opening channels in any of the two locations and for any BH channel. The color version of this figure is available only in the electronic edition.

CONCLUSIONS

Considering the simplicity of implementation and analysis, energy component ratios can provide a valuable tool for network operators as a complement to other diagnostic tools. Our analysis has resulted in metadata (gain) corrections for one GEOSCOPE station and possible update in metadata for other stations. Using this method in conjunction with approaches for updating historical metadata (Xu *et al.*, 2018), it should be possible to retroactively correct metadata for historical time periods as well. In addition, component ratios can also be useful to assess, and directly compare, the performances and

temporal stability of new types of instruments. In the current discussions related to the replacement of the aging STS-1, this can contribute to the assessment of the overall temporal stability of new very broadband sensors.

The implementation we developed aims to show stable results over a wide frequency range and time period. It is also possible to use more simple implementations for network monitoring purposes. For example, GEOSCOPE has now implemented and is routinely running a simple algorithm for calculating daily energy ratios in the period band of 2–10 s without correcting for instrument response, with the objective of continuously monitoring the instruments.

DATA AND RESOURCES

We used data from the GEOSCOPE network, network code G (Institut de Physique du Globe de Paris and École et Observatoire des Sciences de la Terre de Strasbourg [IPGP/EOST], 1982). Station KIP has shared network code IU (Global Seismographic Network [GSN]—Albuquerque Seismological Laboratory/U.S. Geological Survey [ASL/USGS], 1988) and is operated by the Albuquerque Seismological Laboratory, USGS. We downloaded data from the national French seismological data center of Réseau sismologique et géodésique français (RESIF) (seismology.resif.fr) and crosschecked data for KIP by also downloading data from the Incorporated Research Institutions for Seismology (IRIS) Data Management Center (<https://ds.iris.edu/ds/nodes/dmc/>). Software was written using mainly the ObsPy community software package (Krischer *et al.*, 2015). The Python code used to produce the figures of this article is available at https://gricad-gitlab.univ-grenoble-alpes.fr/thollarf/comp_ratio.git, whereas the real-time monitoring code is available at https://github.com/IPGP/geoscope-rms/blob/master/rms_sds.py. All websites were last accessed June 2019. ☒

ACKNOWLEDGMENTS

The authors thank field personnel and data managers who through their dedication make it possible to coherently analyze seismological data spanning several decades. The authors thank Armelle Bernard, Jean-Yves Thoré, and Maxime Bès De Berc for helpful discussions regarding CRZF, DRV, and ECH stations. David Wolyniec from the RESIF data center calculated the probability density functions (PDFs) of Figure 5. The GEOSCOPE network is funded by Centre National de la Recherche Scientifique (CNRS), Institut de Physique du Globe de Paris (IPGP), and Université de Strasbourg. The GEOSCOPE stations in sub-Antarctic and Antarctic regions are managed with support from the French Polar Institute (IPEV) under Program Number 133 “Global Seismological Observatory (SISMOLOGIE/OBS).” The python code used to produce the figures in this article had support to move it to a publishable state from the ISTERre geodata team. The present work received support from the Seismology and Earthquake Engineering Research Infrastructure Alliance for Europe (SERA) project, funded under the European Union’s Horizon 2020 research and innovation program under Grant Agreement Number730900. The authors thank two anonymous reviewers, Jill McCarthy, Janet Slate, and Weiwei Xu for very helpful reviews.

Any use of trade, product, or firm names is for descriptive purposes only and does not imply endorsement by the U.S. Government.

REFERENCES

Albuquerque Seismological Laboratory/U.S. Geological Survey (ASL/USGS) (1988). Global Seismograph Network (GSN - IRIS/USGS), *International Federation of Digital Seismograph Networks. Dataset/Seismic Network*, doi: [10.7914/SN/IU](https://doi.org/10.7914/SN/IU).

- Casey, R., M. E. Templeton, G. Sharer, L. Keyson, B. R. Weertman, and T. Ahern (2018). Assuring the quality of IRIS data with MUSTANG, *Seismol. Res. Lett.* **89**, 630–639.
- Davis, P., and J. Berger (2007). Calibration of the Global Seismographic Network using tides, *Seismol. Res. Lett.* **78**, 454–459.
- Davis, P., and J. Berger (2012). Initial impact of the global seismographic network quality initiative on metadata accuracy, *Seismol. Res. Lett.* **83**, 697–703.
- Davis, P., M. Ishii, and G. Masters (2005). An assessment of the accuracy of GSN sensor response information, *Seismol. Res. Lett.* **76**, 678–683.
- Ekström, G., and M. Nettles (1997). Calibration of the HGLP seismograph network and centroid-moment tensor analysis of significant earthquakes of 1976, *Phys. Earth Planet. In.* **101**, 219–243.
- Ekström, G., C. A. Dalton, and M. Nettles (2006). Observations of time-dependent errors in long-period instrument gain at global seismic stations, *Seismol. Res. Lett.* **77**, 12–22.
- Grob, M., A. Maggi, and E. Stutzmann (2011). Observations of the seasonality of the Antarctic microseismic signal, and its association to sea ice variability, *Geophys. Res. Lett.* **38**, L11302, doi: [10.1029/2011gl047525](https://doi.org/10.1029/2011gl047525).
- Hutt, C. R., and A. T. Ringler (2011). Some possible causes of and corrections for STS-1 response changes in the global seismograph network, *Seismol. Res. Lett.* **82**, 560–571.
- Institut de Physique du Globe de Paris and École et Observatoire des Sciences de la Terre de Strasbourg (IPGP/EOST) (1982). *GEOSCOPE - French Global Network of broadband seismic stations*, doi: [10.18715/GEOSCOPE.G](https://doi.org/10.18715/GEOSCOPE.G).
- Kimura, T., H. Murakami, and T. Matsumoto (2015). Systematic monitoring of instrumentation health in high-density broadband seismic networks, *Earth Planets Space* **67**, no. 55, doi: [10.1186/s40623-015-0226-y](https://doi.org/10.1186/s40623-015-0226-y).
- Krischer, L., T. Megies, R. Barsch, M. Beyreuther, T. Lecocq, C. Caudron, and J. Wassermann (2015). ObsPy: A bridge for seismology into the scientific Python ecosystem, *Comput. Sci. Discov.* **8**, no. 1, 0140, doi: [10.1088/1749-4699/8/1/014003](https://doi.org/10.1088/1749-4699/8/1/014003).
- Langston, Ch. A. (2018). Calibrating dense spatial arrays for amplitude statics and orientation errors, *J. Geophys. Res.* **123**, 3849–3870.
- McNamara, D. E., and R. I. Boaz (2005). Seismic noise analysis system, power spectral density probability density function: Stand-alone software package, *U.S. Geol. Surv. Open-File Rept. No. 2005-1438*, 30 pp.
- Park, S., and M. Ishii (2019). Detection of instrument gain problems based on body-wave polarization: Application to the Hi-Net Array, *Seismol. Res. Lett.* **90**, no. 2A, 692–698.
- Pavlis, G. L., and F. L. Vernon (1994). Calibration of seismometers using ground noise, *Bull. Seismol. Soc. Am.* **84**, 1243–1255.
- Peterson, J. (1993). Observations and modelling of background seismic noise, *U.S. Geol. Surv. Open-File Rept. 93-322*, U. S. Geological Survey, Albuquerque, New Mexico.
- Ringler, A. T., L. S. Gee, C. R. Hutt, and D. E. McNamara (2010). Temporal variations in global seismic station ambient noise power levels, *Seismol. Res. Lett.* **81**, 605–613.
- Ringler, A. T., M. T. Hagerty, J. F. Holland, A. Gonzales, L. S. Gee, J. D. Edwards, D. C. Wilson, and A. Baker (2015). The data quality analyzer: A quality control program for seismic data, *Comput. Geosci.* **76**, 96–111.
- Ringler, A. T., C. R. Hutt, L. S. Gee, L. D. Sandoval, and D. Wilson (2014). Obtaining changes in calibration-coil to seismometer output constants using sine waves, *Bull. Seismol. Soc. Am.* **104**, no. 1, 582–586.
- Ringler, A. T., T. Storm, L. S. Lee, C. R. Hutt, and D. Wilson (2015). Uncertainty estimates in broadband seismometer sensitivities using microseisms, *J. Seismol.* **19**, 317–327.
- Romanowicz, B. (1990). The federation of digital broad band seismic networks, available at http://www.fdsn.org/media/_s/publications/historical/fdsn_report_romanowicz.pdf (last accessed April 2019).
- Romanowicz, B., and A. M. Dziewonski (1987). Global digital seismographic network: Research opportunities and recent initiatives,

- in *Composition, Structure and Dynamics of the Lithosphere-Asthenosphere System*, C. Fuchs and C. Froidevaux (Editors), Geodynamics series, Vol. 16, A.G.U. Publications, 99–110, .
- Roult, G., J.-P. Montagner, B. Romanowicz, M. Cara, D. Rouland, R. Pillot, J.-F. Karczewski, L. Riera, E. Stutzmann, A. Maggi, and the GEOSCOPE team (2010). The Geoscope program: Progress and challenges during the past 30 years, *Seismol. Res. Lett.* **81**, 427–452.
- Tasić, I. (2018). Interdependent quality control of collocated seismometer and accelerometer, *J. Seismol.* **22**, 1595–1612.
- Ueno, T., T. Saito, K. Shiomi, and Y. Haryu (2015). Monitoring the instrument response of the high-sensitivity seismograph network in Japan (Hi-net): Effects of response changes on seismic interferometry analysis, *Earth Planets Space* **67**, no. 135, doi: [10.1186/s40623-015-0305-0](https://doi.org/10.1186/s40623-015-0305-0).
- Woodward, R. L., and G. Masters (1989). Calibration and data quality of the long-period SRO/ASRO networks, 1977 to 1980, *Bull. Seismol. Soc. Am.* **79**, 1972–1983.
- Xu, W., P. Davis, D. Auerbach, and E. Klimczak (2018). Revision of metadata sensitivities at IRIS/IDA stations, *Seismol. Res. Lett.* **89**, 1084–1092.
- Ye, F., J. Lin, Z. Shi, and S. Lyu (2018). Monitoring temporal variations in instrument responses in regional broadband seismic network using ambient seismic noise, *Geophys. Prospect.* **66**, 1019–1036.

Helle A. Pedersen
Université Grenoble Alpes, University of Savoie Mont Blanc
CNRS, IRD, IFSTTAR, ISTerre
38000 Grenoble, France
helle.pedersen@univ-grenoble-alpes.fr

Nicolas Leroy
Martin Vallée
Institut de Physique du Globe de Paris
Université de Paris, CNRS
F-75005 Paris, France

Dimitri Zigone
Institut de Physique du Globe de Strasbourg, UMR 7516
Université de Strasbourg/EOST, CNRS
CS 40700
38058 Grenoble, CEDEX 9
France

Adam T. Ringler
David C. Wilson
U.S. Geological Survey
P.O. Box 82010
Albuquerque, New Mexico 87198-2010 U.S.A.

Published Online 20 November 2019